Research Square

Preprints are preliminary reports that have not undergone peer review.
They should not be considered conclusive, used to inform clinical practice,
or referenced by the media as validated information.

Dynamic Segment-Resolved Modeling of NaOH-H2O Absorption and Desorption in a Falling-Film Heat Exchanger

Stanley Bernauer

stanley.bernauer@hszg.de

Zittau/Görlitz University of Applied Sciences https://orcid.org/0009-0002-0701-0060

Sebastian Braun

Zittau/Görlitz University of Applied Sciences https://orcid.org/0009-0002-8706-8704

Daniel Fiß

Zittau/Görlitz University of Applied Sciences https://orcid.org/0009-0005-5426-6108

Holger Neumann

Zittau/Görlitz University of Applied Sciences https://orcid.org/0000-0002-0683-1353

Manuel Isensee

Zittau/Görlitz University of Applied Sciences https://orcid.org/0009-0001-7901-9884

Alexander Kratzsch

Zittau/Görlitz University of Applied Sciences https://orcid.org/0009-0000-9105-8969

Research Article

Keywords: thermochemical energy storage, falling-film heat exchanger, dynamic process model, sodium hydroxide solution, absorption/desorption, mathematical modeling, heat and mass transfer

Posted Date: April 23rd, 2026

DOI: https://doi.org/10.21203/rs.3.rs-9496847/v1

License: This work is licensed under a Creative Commons Attribution 4.0 International License. Read Full License

Additional Declarations: The authors declare no competing interests.

Dynamic Segment-Resolved Modeling of NaOH–H_2O Absorption and Desorption in a Falling-Film Heat Exchanger

Stanley Bernauer[1], Sebastian Braun[1], Daniel Fiß[1], Holger Neumann[1], Manuel Isensee[1], Alexander Kratzsch[1]

[1]Department of Measurement Technology and Process Automation, Institute of Process Technology, Process Automation and Measurement Technology (IPM), Theodor-Körner-Allee 8, Zittau, 02763, Germany.

Contributing authors: stanley.bernauer@hszg.de;

Abstract

Dynamic models of NaOH–H_2O falling-film absorbers/desorbers are needed for process analysis and future controller design, but time-resolved experimental data for the target system are not yet available. A dynamic segment-resolved model was developed for a horizontal-tube falling-film heat exchanger. Each of the $\boldsymbol{N = 10}$ segments is described by four coupled ordinary differential equations governing inner fluid temperature, wall temperature, external solution mass flow rate, and NaOH mass fraction. Absorption and desorption are represented within a unified framework using mode-dependent heat-transfer assumptions and thermophysical property data for NaOH–H_2O. For absorption, the simulated steady-state concentration change is $\boldsymbol{\Delta w = 0.105}$, close to the reference value of $\boldsymbol{\Delta w = 0.10}$; the small residual deviation is attributed to the surfactant-free operating condition of the model. For desorption, the simulated NaOH concentration of approximately **0.45** lies within the reference range of **0.44** to **0.49**. Energy-balance errors below **0.05 %** confirm the numerical consistency of the implementation. The model yields steady-state results consistent with reported reference values and provides a physically sound dynamic formulation suitable as a preliminary plant model for future model-based control studies. Its primary current limitation is the absence of time-resolved experimental data for transient validation and parameter identification. A sensitivity analysis confirms that the steady-state results are analytically independent of the PT1 time constant $\boldsymbol{\tau}$, and quantifies the strong dependence on $\boldsymbol{\alpha_e}$ and on the number of discretization segments $\boldsymbol{N}$.

Keywords: thermochemical energy storage, falling-film heat exchanger, dynamic process model, sodium hydroxide solution, absorption/desorption, mathematical modeling, heat and mass transfer

1 Introduction

Thermochemical energy conversion processes are gaining increasing importance in the context of renewable energy supply and efficient heat provision. A promising approach exploits the properties of aqueous sodium hydroxide, owing to its elevated boiling point relative to pure water, thermal energy can be transferred to a higher temperature level by means of absorption and desorption processes, enabling compact seasonal heat storage [1–3]. Existing models for such tube systems are confined to steady-state descriptions and are therefore unsuitable for controller design. A dynamic model is required that captures heat and mass transport across the entire system geometry in a time-resolved manner. The objective of this work is to develop such a model that represents temperature, concentration, and phase-change processes realistically as functions of time. Since no time-resolved experimental data are available for the target system, this work is explicitly framed as a model development contribution. The focus is on establishing a physically consistent dynamic formulation and demonstrating agreement with reported steady-state reference values, rather than on quantitative transient validation.

Section 2 surveys the relevant literature and situates the contribution within current research. Section 3 details the modeling methodology, boundary conditions, and model parameters. Section 4 presents the simulation results for both absorption and desorption, together with a sensitivity analysis of the key uncertain parameters. Section 5 interprets these results and outlines limitations and future work. Section 6 draws conclusions.

2 Literature Review

Closed-sorption heat storage based on the working-fluid pair NaOH–H_2O has been studied extensively as a high energy-density alternative to sensible heat storage. Daguenet et al. [4] developed a numerical model for the reaction zone of a 1 kW falling-film laboratory prototype and validated it experimentally for desorption; the experimental concentration changes constitute the primary reference for the present work. Building on these results, Jahnke [5] investigated the related Honigmann process for thermochemical energy storage, providing an additional context for the thermodynamic modeling approach.

Recent studies have extended the scope to system-level and multi-mode analyses. Su et al. [1] proposed a two-stage solar–NaOH thermochemical heat pump for building heating and analyzed a range of operational strategies, demonstrating theoretical coefficients of performance well above those of sensible storage. At the component level, Canela-Sánchez et al. [6] developed and validated a segmented ODE-based model of a helical falling-film evaporator using a PT1 representation for the liquid

film, demonstrating that a tube-by-tube discretization scheme accurately reproduces measured temperature profiles under varying operating conditions. The present work adopts the same general discretization philosophy, but differs in several fundamental respects: the geometry consists of horizontal tubes operating in the discrete droplet flow regime (Re $\approx$ 0.5–8), the working fluid is a chemically reactive sorbent (NaOH solution) whose concentration-dependent boiling point elevation constitutes an additional state variable, and both absorption and desorption modes are modeled within a single unified framework — aspects not addressed by Canela-Sánchez et al. [6].

Padamurthy et al. [7] provide a review of emerging trends in thermochemical energy storage for building heating and hot-water applications, surveying both open and closed-loop sorption systems, including NaOH-based configurations and identifying the limited availability of validated dynamic models as a key obstacle to their wider deployment. A broader perspective is provided by Abdullah et al. [2], who review thermochemical seasonal solar energy storage materials and modeling methods, and by Spietz et al. [3], who survey salt-hydrate thermochemical storage systems and identify key challenges regarding reaction kinetics and cycle stability.

Model-based control of thermochemical energy storage systems has recently gained significant attention. Wei et al. [8] investigated the integration of model predictive control (MPC) with seasonal thermochemical storage in a district heating network, demonstrating that MPC can substantially reduce unmet heating demand by optimizing charge and discharge cycles. At the component level, Rentz et al. [9] developed a dynamic ODE model and subsequently designed an MPC controller for the hydration process in a $CaO/Ca(OH)_2$ thermochemical storage reactor, following the same model-first approach that the present work adopts for the NaOH system.

The present work addresses the identified research gap in dynamic model formulation by providing a fully dynamic, segment-resolved ODE model of both the absorption and desorption modes of a NaOH–H_2O falling-film heat exchanger operating in the horizontal-tube, droplet-flow configuration. As the primary reference dataset provides only steady-state target values [4], the contribution is explicitly scoped as a model development study: steady-state consistency is demonstrated as a necessary condition for physical correctness, while the developed model forms the basis for future model-based control design.

3 Materials and Methods

3.1 Model Description

The object of modeling is the dynamic heat and mass transport in a falling-film heat exchanger containing sodium hydroxide solution. The heat exchanger is discretized into N segments, as illustrated in Figure 1. Each segment n is characterized by the internal fluid temperature $T_{i,n}$, the wall temperature $T_{w,n}$, and the external mass flow rate $\dot{m}_{e,n}$. The working fluid enters at $T_{i,\text{in}}$ and flows from segment 1 to N, while the sorbent enters at segment $N+1$ with mass flow rate $\dot{m}_{e,N+1}$ and exits at segment 1.

For each segment $n \in \{1, \ldots, N\}$, coupled mass and energy balances are established, resulting in a system of ordinary differential equations. Inside the tubes, water flows (index i), while on the outside a film of sodium hydroxide (index e) trickles down

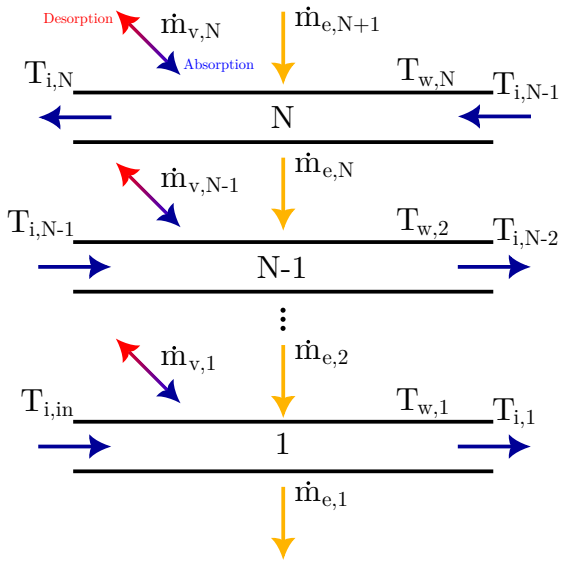


Fig. 1 Discretization scheme of the falling-film heat exchanger with N segments. Yellow: NaOH flow; blue: water flow.

the tube wall. Thermal exchange between the two media occurs across the tube wall (index w) according to Newton's law of cooling [10]. Four state variables describe the system state per segment: inner fluid temperature $T_{i,n}$, wall temperature $T_{w,n}$, external solution mass flow rate $\dot{m}_{e,n}$, and NaOH concentration w_n.

The model considers a clearly separated phase configuration. The water flows inside the tubes, while the liquid NaOH film is located on the external tube surface. Heat transfer occurs through the solid tube wall, whereas mass transfer is restricted to the vapor?liquid interface on the external side. No mass transfer through the solid wall is considered.

3.2 Inner Temperature

The energy balance of the liquid water comprises convective transport through the mass flow $\dot{m}_i$ (const.) and heat transfer to the tube wall. The associated coefficient is $k_{i,n} = \alpha_{i,n} A_i / (m_{i,n} \cdot c_{p_{i,n}})$. For the entry segment ($n = 1$):

$$\frac{\mathrm{d}T_{i,1}(t)}{\mathrm{d}t} = -\left(\frac{\dot{m}_i(t)}{m_{i,1}(t)} + k_{i,1}(t)\right) T_{i,1}(t) + k_{i,1}(t)\, T_{w,1}(t) + \frac{\dot{m}_i(t)}{m_{i,1}(t)}\, T_{i,\mathrm{in}}(t) \qquad (1)$$

In the downstream segments ($n = 2, \ldots, N$), the outlet temperature of the preceding segment replaces the inlet boundary condition:

$$\frac{\mathrm{d}T_{i,n}(t)}{\mathrm{d}t} = \frac{\dot{m}_i(t)}{m_{i,n}(t)}\, T_{i,n-1}(t) - \left(\frac{\dot{m}_i(t)}{m_{i,n}(t)} + k_{i,n}(t)\right) T_{i,n}(t) + k_{i,n}(t)\, T_{w,n}(t) \qquad (2)$$

3.3 Wall Temperature

The tube wall absorbs heat from the inner fluid and transfers it to the external solution film. With $k_{wi,n} = \alpha_{i,n} A_i / (m_w c_{p_{w,n}})$ and $k_{we,n} = \alpha_{e,n} A_e / (m_w c_{p_{w,n}})$, the wall energy balance reads:

$$\frac{\mathrm{d}T_{w,n}(t)}{\mathrm{d}t} = k_{wi,n}(t)\, T_{i,n}(t) - \left(k_{we,n}(t) + k_{wi,n}(t)\right) T_{w,n}(t) + k_{we,n}(t)\, T_{e,n}(t) \quad (3)$$

The heat of absorption/desorption is implicitly accounted for by the coupling of the phase-change mass flux $\dot{m}_{v,n}$ and the solution's equilibrium temperature $T_{\mathrm{sat}}(p, w)$, which incorporates the concentration-dependent boiling point elevation of the NaOH solution.

The heat transfer coefficients $\alpha_{i,n}$ and $\alpha_{e,n}$ are specified based on the respective operating mode and the available experimental boundary conditions of Daguenet et al. [4]. For the inner side, the heat transfer coefficient is computed using standard forced-convection correlations for internal pipe flow as provided in the VDI Heat Atlas [11], based on thermophysical properties and flow-dependent dimensionless numbers. Different closure relations are used for absorption and desorption due to the change in hydrodynamic regime between droplet-driven interfacial contact and film-dominated flow conditions.

- **Desorption:** $\alpha_{e,n}$ is calculated using the classical Nusselt film theory for laminar falling films [11], reflecting the dominant heat transport mechanism during evaporation.
- **Absorption:** Standard analytical correlations for falling-film heat transfer, including those based on Nusselt film theory, are derived for continuous liquid films and are not directly applicable to the discrete droplet flow regime ($\mathrm{Re} \approx 0.5$–8) encountered in the present system. As shown by Killion and Garimella [12], droplet formation, detachment, and impact on horizontal tube absorbers give rise to complex hydrodynamic phenomena that deviate fundamentally from the assumptions underlying smooth-film correlations; Subramaniam and Garimella [13] further demonstrated that coupled heat and mass transfer in such flows involves droplet-driven mixing mechanisms not captured by simple film models. No published correlation has been identified that adequately captures heat transfer in the droplet regime for the concentrated NaOH system on horizontal tubes. A constant value of $\alpha_{e,n} = 250\,\mathrm{W\,m^{-2}\,K^{-1}}$ is therefore adopted, corresponding to the lower bound of the experimentally measured range of 250–400 $\mathrm{W\,m^{-2}\,K^{-1}}$ reported by Daguenet et al. [4] for a geometrically comparable 1 kW falling-film tube bundle at an HTF inlet temperature of 35 °C. This assumption is required due to the absence of validated heat transfer correlations for the droplet-flow regime in the present system. A similar approach has been adopted by Álvarez and Bourouis [14].

The external temperature $T_{e,n}$ represents the mean equilibrium temperature of the NaOH solution within segment n and is approximated as the arithmetic mean of the

saturation temperatures at the segment boundaries:

$$T_{e,n}(t) = \frac{T_{\mathrm{sat}}(p,\, w_n(t)) + T_{\mathrm{sat}}(p,\, w_{n+1}(t))}{2}, \tag{4}$$

where $T_{\mathrm{sat}}(p, w)$ is the concentration-dependent boiling temperature of the NaOH solution at pressure p_e and mass fraction w, obtained from the property library of Olsson et al. [15]. The model assumes local thermodynamic equilibrium at the vapor–liquid interface., For the concentrated solutions considered here ($w \approx 0.45$–0.50), increased solution viscosity may limit liquid-phase mass transfer and thus reduce the validity Range of the equilibrium assumption. Incorporating a finite interfacial mass transfer resistance is therefore identified as a relevant extension for future model refinement.

3.4 Mass Flow Rate of the External Solution

To represent the trickling of sodium hydroxide along the tube wall physically, the external mass flow rate is modeled as a first-order lag element (PT1) with time constant τ. This delay accounts for the finite settling time the liquid film requires after a boundary condition change before reaching the new steady-state flow. The solution traverses the segments counter to the inner fluid flow direction ($N \to 1$); for $n < N$:

$$\frac{\mathrm{d}\dot{m}_{e,n}(t)}{\mathrm{d}t} = \frac{1}{\tau}\,\dot{m}_{v,n}(t) + \frac{1}{\tau}\,\dot{m}_{e,n+1}(t) - \frac{1}{\tau}\,\dot{m}_{e,n}(t) \tag{5}$$

At the inlet of the external solution ($n = N$), the imposed inlet mass flow replaces the downstream contribution:

$$\frac{\mathrm{d}\dot{m}_{e,N}(t)}{\mathrm{d}t} = \frac{1}{\tau}\,\dot{m}_{v,N}(t) + \frac{1}{\tau}\,\dot{m}_{e,N+1}(t) - \frac{1}{\tau}\,\dot{m}_{e,N}(t) \tag{6}$$

The phase-change mass flow $\dot{m}_{v,n}$ describes the mass exchanged between the vapor phase and the liquid film at segment n. By sign convention, $\dot{m}_{v,n} > 0$ denotes mass transfer from the vapor into the liquid film (absorption), and $\dot{m}_{v,n} < 0$ denotes mass transfer from the liquid film to the vapor phase (desorption).

The governing equation of each segment is given by the control-volume energy balance:

$$\alpha_{e,n} A_e (T_{w,n} - T_{e,n}) + \dot{m}_{v,n}\,\Delta h_{v,n} = H_{\mathrm{out},n} - H_{\mathrm{in},n}. \tag{7}$$

Here, $H_{\mathrm{in},n}$ and $H_{\mathrm{out},n}$ denote the sensible enthalpy flow rates of the NaOH solution entering and leaving segment n, respectively, evaluated using the temperature- and concentration-dependent specific enthalpy function $h(T, w)$.

This nonlinear energy balance is solved at each time step using a Newton–Raphson iteration, where $\dot{m}_{v,n}$ is the primary unknown. Within each iteration, thermophysical properties such as enthalpy and vaporization enthalpy $\Delta h_{v,n}$ (obtained from steam tables [16]) are updated consistently.

The interfacial mass flux $\dot{m}_{v,n}$ therefore results from the coupling between latent heat effects and the axial evolution of the liquid-phase enthalpy along the segmented control volumes.

This interfacial mass transfer acts as a source/sink term in the liquid-phase mass balance, thereby modifying the axial evolution of the solution mass flow along the segments.

The time constant $\tau = 2\,\mathrm{s}$ follows Canela-Sánchez et al. [6], who employed the same low-order PT1 representation in a validated segmented ODE model of a helical falling-film evaporator. A physical indication of a relevant time scale for the present system is provided by the wetting time measurements reported by Daguenet et al. [4] for aqueous sodium hydroxide (45 %) flowing over stainless steel tubes of the same geometry. In those experiments, the characteristic time for a droplet to wet and fall from the tube surface was approximately 1–2 s when the surfactant Triton QS-15 was added to the solution. Without surfactant addition — which corresponds to the operating condition of the present model — the same experiments show that droplets remain stable for significantly longer periods, suggesting that $\tau = 2\,\mathrm{s}$ represents a lower bound for the surfactant-free case. The chosen value is therefore to be understood as a conceptual assumption that enables investigation of one possible dynamic behavior; it does not constitute a system-specifically identified parameter, and its reliable determination requires dedicated transient measurements. Importantly, τ governs only the transient trajectory of the system and has no influence on the steady-state equilibrium; the steady-state validation presented in Section 4 is therefore entirely independent of the chosen value of τ.

3.5 Concentration

Consistently with the mass-flow modeling, the NaOH concentration dynamics are also represented by a PT1 element with the same time constant $\tau = 2\,\mathrm{s}$, capturing the inertia of the concentration equalization in the trickling film:

$$\frac{\mathrm{d}w_n(t)}{\mathrm{d}t} = \frac{1}{\tau}\left(\frac{w_{n+1}(t)\,\dot{m}_{e,n+1}(t)}{\dot{m}_{e,n+1}(t) + \dot{m}_{v,n}(t)} - w_n(t)\right), \tag{8}$$

with:

$$\dot{m}_{e,n} = \dot{m}_{e,n+1} + \dot{m}_{v,n},\ \dot{m}_{v,n} > 0 \text{ for absorption and } \dot{m}_{v,n} < 0 \text{ for desorption.} \tag{9}$$

The numerical solution of the resulting ODE system is performed in MATLAB using an implicit, adaptive multi-step method [10, 17]. Physical property data are taken from a NaOH property library [15] and the steam tables [16].

3.6 Boundary Conditions

Following Daguenet et al. [4], a tube arrangement of ten tubes is adopted. The inner diameter is $d_i = 8\,\mathrm{mm}$ at an outer diameter of $d_a = 10\,\mathrm{mm}$; the tube length is $l = 0.2\,\mathrm{m}$ without considering the tube bends. The pressure drop is calculated with a pipe friction coefficient $\zeta = 0.161$ according to the VDI Heat Atlas [11]. The quality criterion is the concentration change Δw; according to Daguenet et al. [4] the expected values are $\Delta w = 0.10$ (absorption) and $\Delta w = 0.15$ (desorption).

The inner fluid pressure is modeled using a Bernoulli-type relation based on the prescribed inlet conditions and gravitational effects. This constitutes a closure assumption for the vapor phase, which is not explicitly resolved in the present one-dimensional formulation. The external pressure is assumed constant and corresponds to the vacuum level specified in the Abstorex setup.

Prior to each step excitation, the model is integrated from an approximate initial state until the residuals of all state variables fall below a relative tolerance of 10^{-6}, thereby establishing a consistent steady-state initial condition.

3.7 Model Parameters

Table 1 consolidates all model parameters, classifying each according to its source (geometric specification, literature correlation, or selected/assumed) and noting the associated uncertainty or comment. This classification makes transparent which parameters are fixed by the reference geometry, which follow established correlations, and which carry the largest uncertainty for future identification work.

Table 1 Summary of model parameters.

Parameter	**Symbol**	**Value**	**Source**	**Type / Uncertainty**
Number of segments	N	10	[4]	Geometric (reference rig)
Inner tube diameter	d_i	8 mm	[4]	Geometric
Outer tube diameter	d_a	10 mm	[4]	Geometric
Tube length	l	0.2 m	[4]	Geometric
Pipe friction coeff.	ζ	0.161	[11]	Literature
PT1 time constant	τ	2 s	[4, 6]	Assumed (transient only)
Ext. HTC (abs.)	α_e	$250\,\mathrm{W\,m^{-2}\,K^{-1}}$	[4]	Selected (low bound)
Ext. HTC (des.)	α_e	Nusselt corr.	[11]	Film theory
Thermo-physical props.	–	library	[15, 16]	Literature
ODE tolerance	–	10^{-6}	–	Numerical

4 Results

4.1 Absorption

The reference for the absorption simulation is Daguenet et al. [4], which reports a concentration change from $w = 0.5$ to $w = 0.4$. Starting from the steady-state operating point, a step change in the external mass flow from $\dot{m}_e = 0.00065\,\mathrm{kg\,s^{-1}}$ to $\dot{m}_e = 0.0005\,\mathrm{kg\,s^{-1}}$ is imposed at $t = 50\,\mathrm{s}$ in order to characterize the transient system behavior. The red dashed lines in Figure 2 indicate the respective boundary condition values.

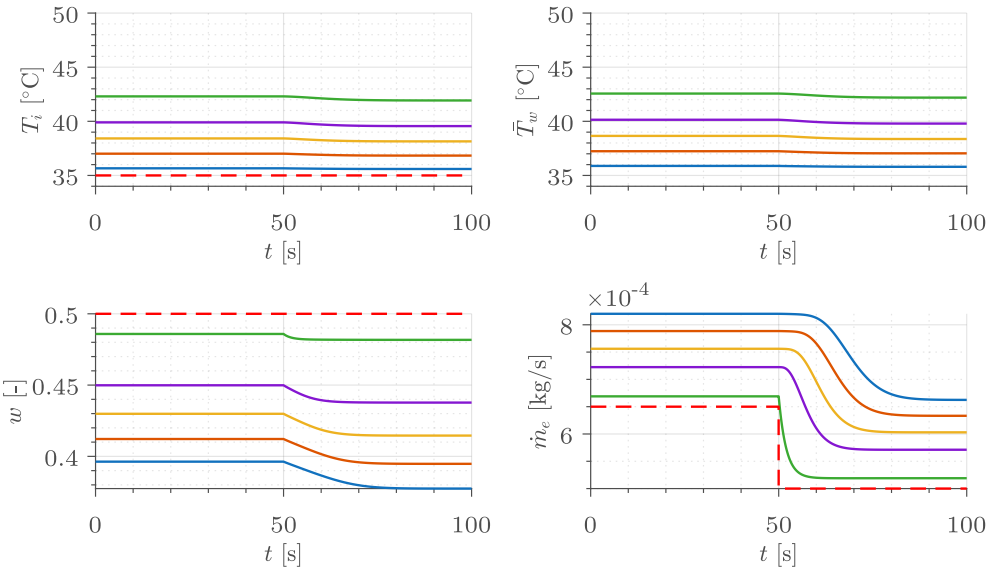


Fig. 2 Simulation results for absorption – step at $t = 50\,\mathrm{s}$; $\dot{m}_e$: $6.5 \times 10^{-4} \rightarrow 5 \times 10^{-4}\,\mathrm{kg\,s^{-1}}$. Solid colored lines represent individual tubes: green – tube 10, purple – tube 7, yellow – tube 5, orange – tube 3, blue – tube 1. T_i: inner fluid outlet temperature of the respective tube segment; T_w: mean wall temperature along the tube; w and $\dot{m}_e$: segment-exit values of concentration and external solution mass flow rate. Red dashed lines: imposed boundary condition values.

Immediately after the mass-flow step, the inner and wall temperatures rise; the increasing temperature rise in the downstream direction (tube 1 to tube 10) confirms the exothermic nature of absorption. Simultaneously, external solution mass flow increases while the concentration drops due to enhanced water-vapor absorption. The shift in thermodynamic equilibrium results in a transition to a new, stable operating point. The simulated steady-state concentration change is $\Delta w = 0.105$, compared with the reference target of $\Delta w = 0.10$ reported by Daguenet et al. [4]. his small deviation of $+0.005$ is within expected experimental uncertainty. The reference experiments were conducted with the surfactant Triton QS-15 to improve wetting conditions. The energy balance closes with a relative error of only 0.0239 %, confirming the numerical consistency of the ODE integration.

4.2 Desorption

For the desorption case, the simulation results are compared with experimental data from Daguenet et al. [4], which documents NaOH concentrations in the range of 44 % to 49 %. To excite the system, the external mass flow is stepped up from $\dot{m}_e = 0.00082$ to $0.0009\,\mathrm{kg\,s^{-1}}$. Red dashed lines in Figure 3 again indicate the boundary condition specifications.

After the imposed step, temperatures and mass flow rise markedly in all segments. Tube 1 exhibits the highest inner temperature while tube 10 shows the coolest state; the temperature difference between inner and wall temperature remains small in all segments. In parallel, the concentration falls in all tubes, with the strongest decrease

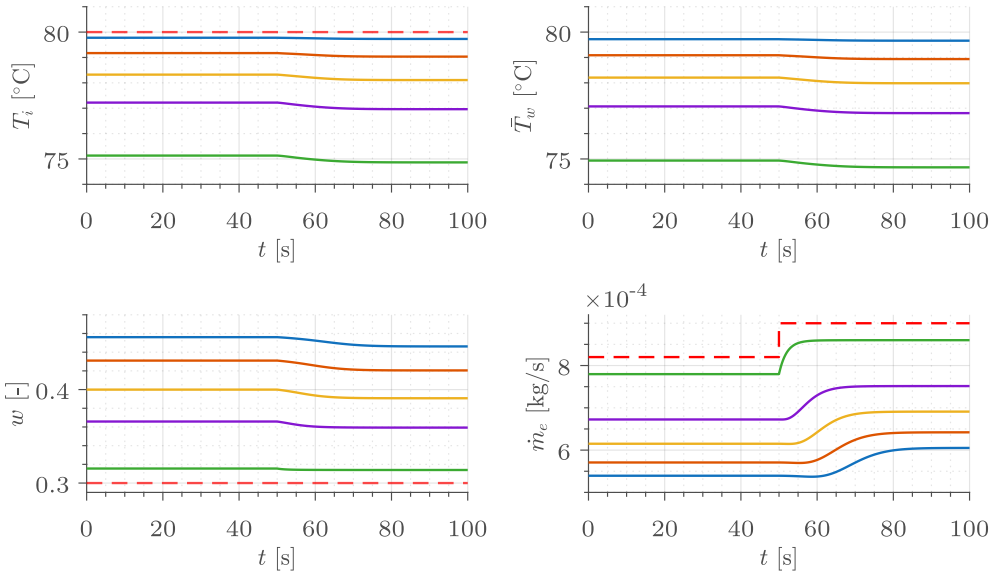


Fig. 3 Simulation results for desorption – mass-flow step $\dot{m}_e$: $8.2 \times 10^{-4} \rightarrow 9 \times 10^{-4}\,\mathrm{kg\,s^{-1}}$. Solid colored lines represent individual tubes: green – tube 10, purple – tube 7, yellow – tube 5, orange – tube 3, blue – tube 1. T_i: vinner fluid outlet temperature; T_w: mean wall temperature; w and $\dot{m}_e$: segment-exit values. Red dashed lines: imposed boundary condition values.

in tube 10, reflecting the greatest water loss through desorption at that location. The synchronous, oscillation-free behavior of all segments indicates a numerically stable simulation. The simulated steady-state NaOH concentration reaches approximately $w \approx 45\,\%$, which lies within the reference range of 44 % to 49 % reported by Daguenet et al. [4]; the corresponding concentration change $|\Delta w| = 0.15$ is consistent with the reference target summarized in Table 2. The energy balance closes with a relative error of 0.0494 %, confirming numerical consistency for this operating mode as well.

4.3 Summary of Simulation–Reference Comparison

Table 2 summarizes the key simulation outputs against the reference values from Daguenet et al. [4].

Table 2 Comparison of simulated results with reference values from Daguenet et al. [4]. Energy balance errors confirm numerical consistency; the deviation in Δw for absorption is discussed in Section 4. Sensitivity of the steady-state results to the key uncertain parameters (τ, α_e, N) is assessed in Section 4.4.

Quantity	**Ref. [4]**	**Simulation**	**Dev.**
Δw absorption (steady state)	≈ 0.10	0.105	+0.005
Δw desorption (steady state)	0.15	0.15	0
Energy balance error, absorption	–	0.0239 %	–
Energy balance error, desorption	–	0.0494 %	–

4.4 Sensitivity Analysis

Three model parameters carry the most uncertainty (see Table 1): the PT1 time constant τ, the external heat-transfer coefficient α_e (absorption only), and the number of discretization segments N. Their influence on the steady-state results is assessed below.

Sensitivity to τ.

The PT1 time constant τ enters the model solely as a common factor in the mass-flow and concentration differential equations (Eqs. 5–8). At steady state all time derivatives vanish:

$$0 = \frac{1}{\tau}\,\dot{m}_{v,n} + \frac{1}{\tau}\,\dot{m}_{e,n+1} - \frac{1}{\tau}\,\dot{m}_{e,n} \quad \Longrightarrow \quad \dot{m}_{e,n} = \dot{m}_{e,n+1} + \dot{m}_{v,n}. \tag{10}$$

Since τ appears as a common prefactor on both sides, it cancels identically from every steady-state balance equation. The steady-state values of all state variables – and therefore Δw – are consequently *analytically independent* of τ. The only quantity governed by τ is the transient settling time: a larger τ prolongs the approach to equilibrium without altering the equilibrium itself.

Sensitivity to α_e.

For absorption, α_e is the primary uncertain parameter; it directly scales the wall-to-film heat flux that drives the phase-change mass flow $\dot{m}_{v,n}$ and hence Δw. Figure 4 shows the simulation with $\alpha_e = 400\,\mathrm{W\,m^{-2}\,K^{-1}}$ (upper bound of the experimental range [4]) using the same boundary conditions as the base case. The exit concentration of tube 1 settles at $w \approx 0.32$, yielding $\Delta w \approx 0.18$ – nearly double the reference value of $\Delta w = 0.10$. This confirms a strong monotonic dependence: increasing α_e within the measured range from 250 to $400\,\mathrm{W\,m^{-2}\,K^{-1}}$ drives Δw from 0.105 to 0.18. The base case ($\alpha_e = 250\,\mathrm{W\,m^{-2}\,K^{-1}}$) already slightly overshoots the reference; adopting the upper bound would substantially worsen agreement. This validates the lower experimental bound as the physically appropriate choice for the surfactant-free operating condition and demonstrates that the model is sensitive to this parameter in the physically expected direction. System-specific identification of α_e from transient measurements therefore remains the highest-priority experimental objective.

Sensitivity to N.

The base case uses $N = 10$ segments, matching the tube count of the reference apparatus [4]. Figures 5 and 6 show the corresponding results for $N = 5$. For absorption ($\alpha_e = 250\,\mathrm{W\,m^{-2}\,K^{-1}}$, same boundary conditions), tube 1 (blue) settles at $w \approx 0.42$, yielding $\Delta w \approx 0.08$ – below both the reference value and the $N = 10$ result of 0.105. For desorption, the exit concentration (tube 1, blue) reaches approximately $w \approx 0.38$–0.39, compared with $w \approx 0.45$ for $N = 10$. In both modes the reduced discretization underestimates the total concentration change because each segment accumulates less heat and mass transfer per unit path length when fewer but longer segments are used. The $N = 10$ discretization, which corresponds to a one-segment-per-tube resolution,

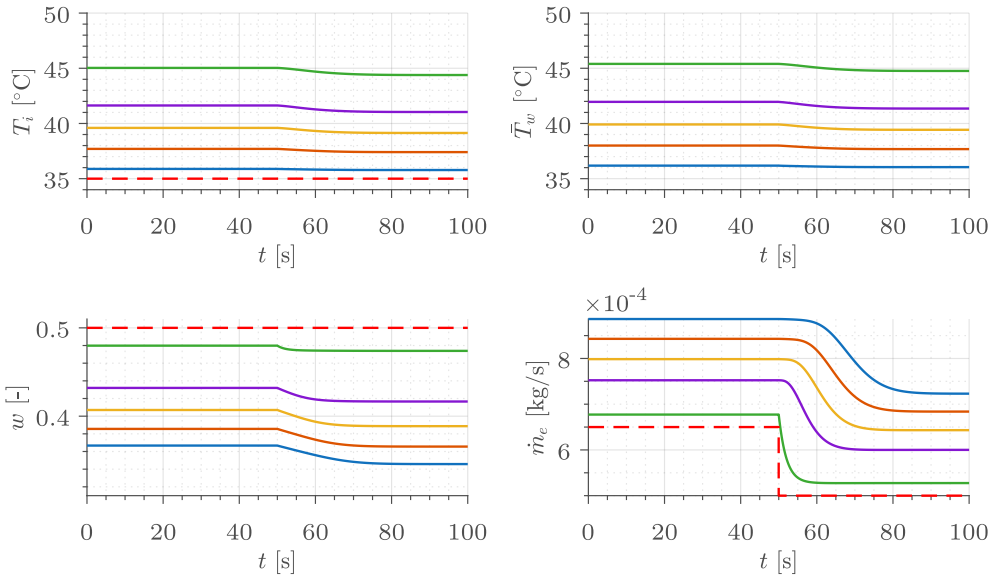


Fig. 4 Absorption simulation with $\alpha_e = 400\,\mathrm{W\,m^{-2}\,K^{-1}}$ (upper bound of the experimental range [4]), $N = 10$ segments, step at $t = 50\,\mathrm{s}$; $\dot{m}_e$: $6.5 \times 10^{-4} \rightarrow 5 \times 10^{-4}\,\mathrm{kg\,s^{-1}}$. Tube 1 (blue) exits at $w \approx 0.32$, giving $\Delta w \approx 0.18$, compared with $\Delta w = 0.105$ for $\alpha_e = 250\,\mathrm{W\,m^{-2}\,K^{-1}}$ and the reference target of $\Delta w = 0.10$ [4]. Line colors as in Figure 2.

is therefore the physically well-motivated choice; coarser resolutions systematically underpredict the reference values. A systematic grid-convergence study for $N > 10$ is identified as a subject for future work; the present sensitivity analysis already quantifies the strong dependence of the results on N and flags it as a key uncertainty.

Table 3 summarizes the steady-state Δw results across all sensitivity runs.

Table 3 Summary of sensitivity study results. Base case: $N = 10$, $\alpha_e = 250\,\mathrm{W\,m^{-2}\,K^{-1}}$.

Mode	Parameter	Value	Result	Remark
Absorption	α_e	$250\,\mathrm{W\,m^{-2}\,K^{-1}}$	$\Delta w = 0.105$	Base case
Absorption	α_e	$400\,\mathrm{W\,m^{-2}\,K^{-1}}$	$\Delta w \approx 0.18$	Overshoot observed
Absorption	N	5	$\Delta w \approx 0.08$	Underprediction
Absorption	N	10	$\Delta w = 0.105$	Base case
Desorption	N	5	$w_{\mathrm{exit}} \approx 0.38$–$0.39$	Lower than base
Desorption	N	10	$w_{\mathrm{exit}} \approx 0.45$	Base case

5 Discussion

The proposed segmented ODE model reproduces steady-state concentration results in both operating modes that are consistent with the reference data from Daguenet

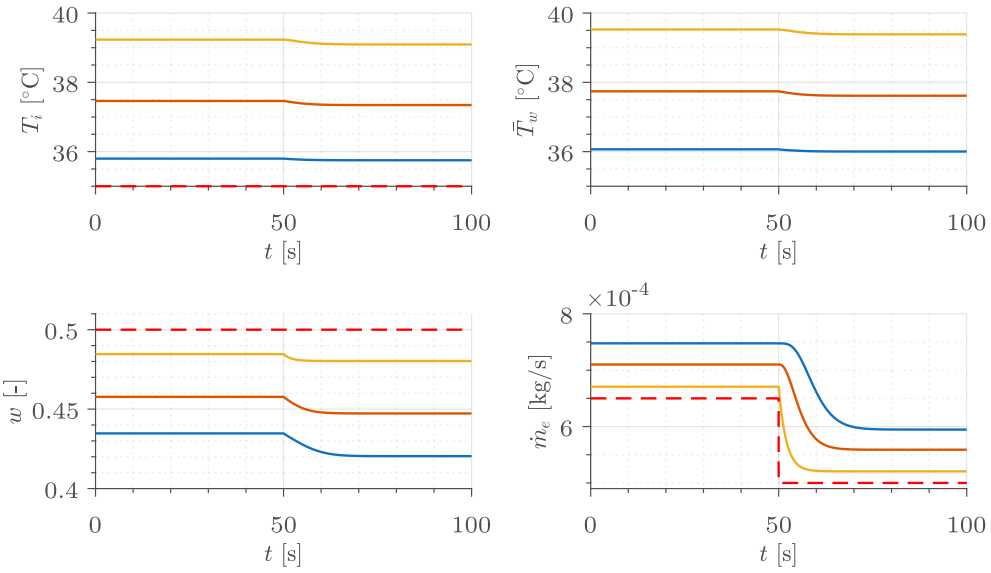


Fig. 5 Absorption simulation with $N = 5$ segments, $\alpha_e = 250\,\mathrm{W\,m^{-2}\,K^{-1}}$, step at $t = 50\,\mathrm{s}$; $\dot{m}_e$: $6.5 \times 10^{-4} \rightarrow 5 \times 10^{-4}\,\mathrm{kg\,s^{-1}}$. Displayed tubes: 5 (yellow), 3 (orange), 1 (blue); red dashed: boundary conditions. Tube 1 exits at $w \approx 0.42$ ($\Delta w \approx 0.08$), below the $N = 10$ result and the reference target.

et al. [4] (see Table 2). This agreement constitutes a necessary condition for physical consistency of the model, but does not represent a full dynamic validation due to the absence of time-resolved experimental data.

For absorption, the simulated concentration change of $\Delta w = 0.105$ slightly exceeds the reference value of 0.10. This deviation is physically plausible and can be attributed to differences in wetting conditions, as the reference experiments employed Triton QS-15 to enhance film stability, whereas the present model assumes surfactant-free operation, which alters interfacial contact and effective mass transfer area. For desorption, the predicted steady-state concentration of approximately 0.45 lies within the reported reference range of 0.44–0.49.

Due to the lack of transient experimental measurements for the investigated system, the present comparison is limited to steady-state observables. Within this constraint, the observed agreement provides a necessary but not sufficient validation of the dynamic model structure. Acquisition of time-resolved data is therefore identified as the most important step for future model verification.

The PT1 representation of the falling film is a lumped approximation of distributed transport processes, which exhibit finite response times due to convection and diffusion [18]. The time constant $\tau = 2\,\mathrm{s}$ is introduced as a conceptual parameter to explore a representative dynamic time scale; it is not system-identified. As shown in Section 3, τ influences only transient trajectories, while steady-state solutions remain unaffected. The consistency of steady-state results therefore provides a robustness check independent of this assumption.

Experimental wetting time data from Daguenet et al. [4] indicate characteristic times of approximately 1–2 s for surfactant-assisted operation. In the absence of

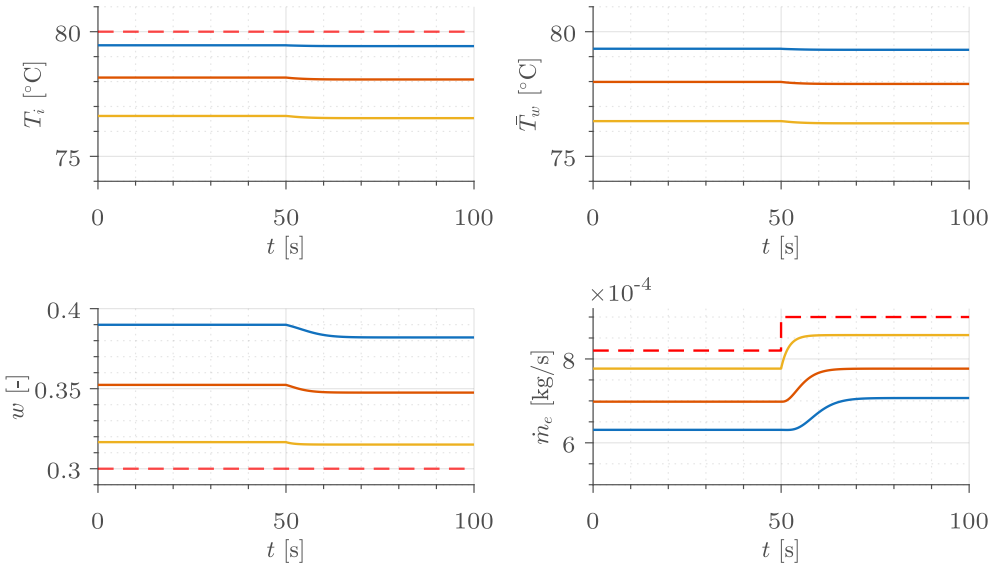


Fig. 6 Desorption simulation with $N = 5$ segments, step at $t = 50\,\mathrm{s}$. Displayed tubes: 5 (yellow), 3 (orange), 1 (blue); red dashed: boundary conditions. Tube 1 exits at $w \approx 0.38$–0.39, compared with $w \approx 0.45$ for $N = 10$.

surfactant, droplet stability increases, implying that the chosen value of $\tau = 2\,\mathrm{s}$ should be interpreted as a lower-bound estimate for surfactant-free conditions. Furthermore, the flow regime at the investigated conditions ($\mathrm{Re} \approx 0.5$–8) corresponds to a droplet-dominated regime, introducing additional uncertainty in the interpretation of a film-based time constant.

Heat transfer coefficients $\alpha_{i,n}$ and $\alpha_{e,n}$ are subject to comparable uncertainties. Classical falling-film correlations, including Nusselt-type formulations, are derived for continuous films and are not directly applicable to the present droplet regime [12, 13]. No validated correlation for concentrated NaOH systems in horizontal droplet-flow tube bundles has been identified. The adopted value of $\alpha_e = 250\,\mathrm{W\,m^{-2}\,K^{-1}}$ is taken from the lower bound of the experimentally reported range by Daguenet et al. [4] and provides the best agreement with the observed concentration change. Similar parameter-based approaches have been used by Álvarez and Bourouis [14] for related systems.

Energy balance errors of 0.0239 % (absorption) and 0.0494 % (desorption) confirm numerical consistency and indicate the absence of significant integration drift. The present model therefore provides a physically consistent dynamic framework at the level of a first-principles ODE formulation, albeit without full experimental transient validation.

The obtained concentration ranges are consistent with values reported for NaOH-based thermochemical storage systems in the literature [1, 2]. However, predictive validation across different geometries and operating conditions remains an open task requiring dedicated experimental datasets.

The observed dependence on the number of segments N indicates a discretization sensitivity rather than a physical effect. The chosen value N = 10 corresponds to the physical tube segmentation but does not guarantee numerical convergence, which should be addressed in future work through a formal grid independence study.

Finally, degradation effects and reaction kinetics, identified as critical limitations in thermochemical storage systems [3], are not yet included in the present formulation and represent a relevant extension for future work, particularly for long-term cycle simulations.

6 Conclusions

The presented work develops a fully dynamic, segment-resolved ODE model for a NaOH–H_2O falling-film heat exchanger, enabling time-dependent simulation of coupled heat and mass transfer in both absorption and desorption modes.

Due to the absence of time-resolved experimental data for the target system, the model shows agreement with available steady-state reference data, providing a first consistency check within the limitations of the dataset, reported by Daguenet et al. [4]. The model reproduces the expected concentration changes with good agreement for both operating modes and maintains strict energy conservation with errors below 0.05%.

A key result is that the steady-state solution is analytically independent of the PT1 time constant τ, confirming that the transient formulation does not affect equilibrium predictions. Sensitivity analysis further shows that the external heat transfer coefficient α_e and the spatial discretization N are the dominant parameters influencing model accuracy.

The model provides a physically consistent and numerically robust basis for future work, including transient experimental identification, parameter estimation, and model-based control design.

Acknowledgements. This work was funded by the German Federal Ministry for Economic Affairs and Energy (BMWi) and the Federal Office for Economic Affairs and Export Control (BAFA) under grant number 46SKD019B. Claude (Anthropic, claude.ai) and ChatGPT (OpenAI, chatgpt.com) were used as a supporting tool during the preparation of this manuscript (language editing and structuring of the literature review). All scientific content, model development, simulation results, and conclusions are the sole responsibility of the authors.

Declarations

- **Funding** This work was funded by the German Federal Ministry for Economic Affairs and Energy (BMWi) and the Federal Office for Economic Affairs and Export Control (BAFA) under grant number 46SKD019B.
- **Conflict of interest** The authors declare no conflict of interest.
- **Ethics approval** Not applicable.
- **Data availability** The datasets generated and/or analysed during the current study are available from the corresponding author upon reasonable request.

- **Code availability** The code used for the numerical model is available from the corresponding author upon reasonable request.
- **Author contribution** Stanley Bernauer conceived the study, developed the model, performed the simulations, and wrote the manuscript. Sebastian Braun, Daniel Fiß, Holger Neumann and Manuel Isensee provided scientific supervision and methodological guidance. Prof. Dr.-Ing. Alexander Kratzsch provided project management and supervision. All authors reviewed and approved the final manuscript.

Abbreviations.

MPC	Model Predictive Control
ODE	Ordinary Differential Equation
PT1	First-order lag element
NaOH	Sodium hydroxide
HTC	Heat transfer coefficient
HTF	Heat transfer fluid

References

[1] Su, Y., Yang, Y., He, G., Liu, R., Ding, D.: Two-stage solar–NaOH thermochemical heat pump heating system for building heating: Operations strategies and theoretical performance. Energies **17**(8), 1976 (2024) https://doi.org/10.3390/en17081976

[2] Abdullah, Koushaeian, M., Shah, N.A., Chung, J.D.: A review on thermochemical seasonal solar energy storage materials and modeling methods. International Journal of Air-Conditioning and Refrigeration **32**(1) (2024) https://doi.org/10.1007/s44189-023-00044-6

[3] Spietz, T., Fryza, R., Lasek, J., Zuwała, J.: Thermochemical energy storage based on salt hydrates: A comprehensive review. Energies **18**(10), 2643 (2025) https://doi.org/10.3390/en18102643

[4] Daguenet, X., Gantenbein, P., Dudita, M., Omlin, L.: ABSTOREX – absorption storage experiment: Final report. Technical report, SPF Institute for Solar Technology, HSR University of Applied Sciences Rapperswil, Rapperswil, Switzerland (2019). Swiss Federal Office of Energy (SFOE) Project SI/501232-01

[5] Jahnke, A.: Untersuchung des Honigmann-prozesses zur thermochemischen energiespeicherung. PhD thesis, Technische Universität Berlin (2019). https://doi.org/10.14279/depositonce-8201

[6] Canela-Sánchez, I.J., Juárez-Romero, D., Escobar-Jiménez, R.F.: Modeling and simulation of a helical falling-film evaporator to improve its performance and design. Applied Thermal Engineering **228**, 120445 (2023) https://doi.org/10.1016/j.applthermaleng.2023.120445

[7] Padamurthy, A., Gandla, P.K., Sheelwant, A., Vemanaboina, H., Paramasivam, P., Ayanie, A.G.: Emerging trends and future prospects of thermochemical energy

storage systems for building space and water heating applications. International Journal of Energy Research, 6685290 (2025) https://doi.org/10.1155/er/6685290 . Article ID 6685290

[8] Wei, Z., Tien, P.W., Calautit, J., Darkwa, J., Worall, M., Boukhanouf, R.: Investigation of a model predictive control (MPC) strategy for seasonal thermochemical energy storage systems in district heating networks. Applied Energy **376**, 124164 (2024) https://doi.org/10.1016/j.apenergy.2024.124164

[9] Rentz, A., Sourmelis, V.E., Kühl, V., Schmidt, M., Linder, M., Sawodny, O.: Model predictive control of the hydration process in a lime-based thermochemical energy storage system. Journal of Dynamic Systems, Measurement, and Control **148**(3), 031006 (2025) https://doi.org/10.1115/1.4070143

[10] Kreyszig, E.: Advanced Engineering Mathematics, 10th edn. Wiley, Hoboken, NJ, USA (2011)

[11] VDI-Gesellschaft Verfahrenstechnik und Chemieingenieurwesen (ed.): VDI-Wärmeatlas, 12th edn. Springer, Berlin (2019)

[12] Killion, J.D., Garimella, S.: Simulation of pendant droplets and falling films in horizontal tube absorbers. Journal of Heat Transfer **126**(6), 1003–1013 (2004) https://doi.org/10.1115/1.1833364

[13] Subramaniam, V., Garimella, S.: From measurements of hydrodynamics to computation of species transport in falling films. International Journal of Refrigeration **32**(4), 607–626 (2009) https://doi.org/10.1016/j.ijrefrig.2009.02.008

[14] Álvarez, M.E., Bourouis, M.: Modelling of coupled heat and mass transfer in a water-cooled falling-film absorber working with an aqueous alkaline nitrate solution. Energies **14**(7), 1804 (2021) https://doi.org/10.3390/en14071804

[15] Olsson, R., Kaarebring-Olsson, M., Jonsson, S.: A Chemical Heat Pump. International Patent WO 97/13267. NaOH–H_2O property data library (1997)

[16] Kretzschmar, H.-J., Wagner, W.: International Steam Tables: Properties of Water and Steam Based on the Industrial Formulation IAPWS-IF97, 3rd edn. Springer, Berlin, Heidelberg (2019). https://doi.org/10.1007/978-3-662-53219-5

[17] Moler, C.: Numerical Computing with MATLAB. SIAM, Philadelphia, PA, USA (2013)

[18] Bird, R.B., Stewart, W.E., Lightfoot, E.N.: Transport Phenomena, 2nd edn. John Wiley & Sons, Hoboken, NJ, USA (2002)